Available online at www.sciencedirect.com
SCIENCE DIRECT®
Composites Science and Technology 66 (2006) 1336–1347
COMPOSITES SCIENCE AND TECHNOLOGY
www.elsevier.com/locate/compscitech

A new composite structure impact performance assessment program ☆

Paolo Feraboli [a,*], Keith T. Kedward [b,1]

[a] Department of Aeronautics and Astronautics, Box 352400, University of Washington, Seattle, WA 98195-2400, United States
[b] Department of Mechanical Engineering, University of California at Santa Barbara, CA 93106, United States

Received 2 June 2005; accepted 27 September 2005
Available online 14 November 2005

Abstract

While previous researchers have conducted their study on the relative impact performance of composite structures from a force or an energy standpoint only, this proposed Composite Structure Impact Performance Assessment Program (CSIPAP) suggests a multi-parameter methodology to gain further insight in the impact behavior of composite structures. These are peak and critical force; critical and dissipated energy; contact duration and coefficient of restitution (COR), which is direct indication of effective structural stiffness; and residual stiffness (normalized contact duration) which yields a plot that bears a striking resemblance with the normalized Compression After Impact (CAI) strength. Using a determinate impactor/target system as baseline configuration, the program is applied toward the understanding of the role played in an impact event by fundamental impactor and target parameters. The equations previously derived for the prediction of the force–energy and residual stiffness curves are shown to apply to the configurations tested, thus confirming their general validity. A modification to the existing effective structural stiffness formulation, which does not account for impactor characteristics, is proposed, and it comprises the impactor material, size and mass characteristics.

Keywords: B. Impact behavior; Damage resistance; C. Damage tolerance; C. Delamination

1. Introduction

1.1. Purpose of the research

An extensive literature review has indicated that many questions still surround the impact response of composite plates. Particularly the ongoing debate on whether a force or energy based criterion should be used to compare impact test results on different configurations, and whether force or energy should be employed to uniquely and satisfactorily assess the state of damage in the composite target. Interesting phenomena were observed in [1–3] in the attempt to address these issues, and a new methodology is here suggested in order to fully benefit of all the information available from an impact test.

The present research has the double purpose of proving the importance of characterizing the impact performance of a composite target by means of multiple parameters, as suggested in this new Composite Structures Impact Performance Assessment Program (CSIPAP), as well as of verifying its validity by applying it to specific parametric studies in order to determine the influence of test configurations on the impact response of composite structures. The proposed CSIPAP is based on the simultaneous analysis of five plots, namely the Force, Energy, Coefficient of Restitution (COR), Contact Duration and Residual Stiffness plots, to fully and satisfactorily address the relative impact performance of composite targets.

In order to build these plots, a specific test matrix has to be employed. It is constituted of three consecutive impact tests, which are performed on each specimen and for each structural configuration. These three tests are, in chrono-

☆ The first part of the research was published in the AIAA Journal 42/10, 2004, while the overall research was awarded the "2004 American Society for Composites Ph.D. Research Award".

* Corresponding author. Tel.: +1 206 543 2170; fax: +1 206 543 0217.
E-mail addresses: feraboli@aa.washington.edu (P. Feraboli), kedward@engineering.ucsb.edu (K.T. Kedward).
[1] Tel.: +1 805 893 3381.

0266-3538/$ - see front matter © 2005 Elsevier Ltd. All rights reserved.
doi:10.1016/j.compscitech.2005.09.009

logical order, subcritical, supercritical and again subcritical in nature. The importance of the first test is to record the pristine contact duration and COR of an elastic impact event, which gives a direct measure of the effective structural stiffness of the target. The second test, which has to be performed at different impact energy levels, has the significance of introducing a progressively increasing amount of damage in the specimen. This test allows for the recording of the critical and peak force values, the critical and dissipated energy values, as well as contact duration and COR. The third and last test, which is again elastic in nature, has the purpose of recording the postfailure (damaged) contact duration of the impulse. Altogether the data thus collected enables the building of the five plots that characterize this proposed CSIPAP, which fully characterizes the impact behavior of a particular structure, and supply the means for an effective parametric investigation.

A summary of the nomenclature previously introduced and used in the present discussion is given:

- Impact energy – impactor's incident kinetic energy introduced in the plate.
- Peak force – maximum recorded load.
- Critical force – value of the load at which a first change of stiffness in the material occurs, also denoted as delamination threshold.
- Critical energy – value of the impact energy corresponding to the critical force.
- Dissipated energy – amount of energy dissipated in damage mechanisms and therefore not restituted to the rebounding impactor.
- Coefficient of restitution – ratio of exit to impact velocities or, equivalently, ratio of the square root of exit to impact energies.
- Total contact duration – resident time of the impactor on the target.
- Subcritical (or elastic) impact events – range of impact energy values below damage threshold.
- Supercritical impact events – range of impact energy values above threshold.

The great advantage of using a multi-parameter approach rather than a single metric to characterize the impact damage resistance and tolerance of a composite target is dual. First, the use of all five plots allows for corroborating and strengthening the otherwise individual conclusions deriving by the use of a single parameter, and more importantly, some conclusions are more readily available for interpretation in a particular plot rather than in another one.

1.2. Literature review

Numerous studies on low velocity impact events on analogous composite systems have been conducted to investigate the effect of boundary conditions, impactor weight, laminate thickness, aperture shape and size, among others. These parametric investigations on different material systems or structural configurations have nonetheless been limited to the use of two criteria only, force and energy. The energy based criterion is comprised of the so-called damage maps, which are plots of damage area vs. impact energy or dissipated energy, and Compression After Impact (CAI) curves, which are plots of the static residual strength vs. impact or dissipated energy. The force criterion relies on the peak force recorded during an impact event to assess the relative performance of different structural configurations.

Jackson and Poe [4] investigated the variation in contact force for two values of laminate thickness, support span and boundary conditions. They concluded that, keeping the other parameters constant, the thicker laminate and smaller aperture gave nearly 50% higher responses, while the fully clamped support gave only a 20% higher response than the simple support.

Nettles and Douglas [5] investigated the relative response of three support span/laminate thickness (s/t) ratios, both in clamped and simply supported conditions. They concluded that boundary conditions appear to have no effect on the peak force (or maximum load) vs. delamination area plot, as well as little effect on stiffness and impulse duration. On the other hand the different s/t ratio gave rise to different load–displacement and load–time curves.

Ambur and Kemmerly [6] plotted the effect of impactor mass on the contact force vs. impact energy curve, showing highly non-linear and unpredictable trends, but concluded that higher impactor masses result in decreasing damage areas. Prasad et al. [7] showed that the contact force recorded for specimens with partially clamped boundary conditions is 24% higher than for the purely supported conditions. In addition, varying impactor weight seems to have small influence on the peak recorded force, yet contact duration is greatly affected by it. Ambur et al. [8] concluded that the effect of impactor size and material on airgun propelled and drop weight impact tests is very different. Increasing impactor size and mass has the effect of decreasing the contact force and increasing the contact duration. Furthermore, airgun-propelled impacts are localized in nature, hence unlike drop weight test independent of support size. Similar conclusions were reached by Delfosse et al. [9] and Li et al. [10], who showed that a lower-mass, higher-velocity impactor leads to a higher stiffness and peak force, and lower maximum displacement and damage extent than a higher-mass, lower velocity impactor for the same value of impact energy.

Sjoblom et al. [11,12] and later Zhou [13] concluded that the delamination initiation force is strictly related to laminate thickness but is independent of the support span. They observed that larger plates absorb more energy and carry higher loads at the same energy level than smaller plates. Zhou also determined that the normalized Compression After Impact (CAI) strength curves of laminates with different thicknesses are virtually identical, thus suggesting

that while laminate thickness plays a fundamental role in damage resistance, its influence is negligible in damage tolerance (residual performance).

Liu et al. [14] employed a multi-parameter methodology to interpret the results and determine the perforation threshold of their targets. The peak force plot shows a transition from a non-linear curve to a straight line (plateau) at the perforation level of impact energy; the contact duration plot shows a quadratic increase up to perforation, which is followed by a sharp drop; the absorbed energy plot shows an initial quadratic trend which then becomes linear at perforation; the compression after impact (CAI) tests revealed that the normalized maximum load decreases from unity to about 50% of the pristine value at perforation, then plateaus around it for higher levels of impact energy.

In their investigation on quasi-isotropic beam specimens, Lifschiz et al. [15] introduce the concept of a 3-test sequence to determine the pristine and damaged values of transverse stiffness. The first and third subcritical tests are employed to record total contact duration, which is directly related to effective structural stiffness, while the second critical test is used to introduce damage in the structure. To quantify the residual performance they plot the relative loss in impact energy, which is linearly related to the relative reduction in beam rigidity.

Kistler and Waas [16] determined that increasing the thickness of the composite target and changing the boundary conditions from simply supported to fully clamped has the effect of increasing the peak recorded force and decreasing the maximum displacement and contact duration.

2. Experimental setup

The laminates used are obtained by hand lay-up of AS4/NCT301 prepreg tape, then press molded at 300 °F (149 °C) for 30 min at 3 bars pressure. The stacking sequence is quasi-isotropic of the form $[0/90/\pm 45]_{ns}$, with $n = 2$–5; the reference laminate is a 32 ply ($n = 4$) with nominal thickness of 0.145 in. (3.68 mm). The unidirectional lamina elastic properties as well as the quasi-isotropic laminate elastic and strength properties can be found in [2].

From the cured panel, square plates of nominal length 6 in. (152.4 mm) are cut with a diamond coated tip disk saw. The reference fixture built for impact as well as static testing [1], is comprised of two steel plates having a 2.5 in. (63.5 mm) diameter circular aperture, which are clamped together by four screws located at the periphery of the composite target. The other fixture employed is identical but has a 5 in. square aperture. For the reference configuration, the composite plate is situated between the two steel plates and is positioned over the aperture with the aid of three locating pins; the 4 screws are then tightened to provide clamped boundary conditions. Testing is also performed by removing the screws and face-plate to provide purely supported boundary conditions, and investigate the effectiveness of clamping mechanisms. The instrumented drop tower is a GRC Dynatup© model 8250, and the software used for data recording/analysis is the 930 version. Impactor carriage weight for the reference configuration is 9.92 lbs (4.51 kg), while the other weight tested is 20.4 lbs (9.27 kg). The striker, or tup, is machined from a 6061-T6 aluminum cylinder with a 1.5 in. (38.1 mm) diameter hemispherical end. Maximum drop height is 34 in. (0.863 m), which yields impact velocities up to 13.9 ft/s (4 m/s) and impact energy levels up to 56 ft lb (75.92 J). The experimental setup used in the present investigation is similar in nature to the one used by many previous researchers, and a summary is provided in Table 1. Table 2 summarizes the eight configurations tested. Due to the

Table 1
Summary of typical low velocity impact test setup and specimen geometry

	Materials	Stacking sequence	No. plies	Type target	Support span in. (mm)	Boundary conditions	Impactor diameter in. (mm)	Impactor mass lb (kg)
Present	AS4/NCT301	$[0/90/\pm 45]_{ns}$	$n = 2$–5	Circ.	2.5 (63.5)	CC	1.5 (38.1)	9.92 (4.50)
				Sqr.	5 (127)	SS		20.4 (9.26)
[3]	AS4/3501-6	$[45/0/-45/90]_{ns}$	$n = 3,6$	Sqr.	5 (127)	SS	0.5 (12.7)	10.18 (4.63)
	IM7/8551-7				8 (203.2)	CC		
[4]	IM7/8552	$[45/90/-45/0]_{ns}$	$n = 1$–6	Sqr.	2–12 (50.8–304.8)	SS	–	–
						CC		
[10]	AS4/3502	$[45/90/-45/0]_{ns}$	$n = 1$–6	Circ.	1–4 (25.4–101.6)	–	–	–
[22]	AS4/3501-6	$[0/90/\pm 45]_{ns}$	$n = 4,5$	Sqr.	10 (254)	CC	0.5 (12.7)	9.46 (4.3)
[5–7]	AS4/3502	$[45/0/-45/90]_{ns}$	$n = 3$–6	Sqr.	5×5 (127×127)	SS/CC	0.5 (12.7)	2.5–20 (1.13–9.07)
	IM7/5260			Rect.	5×10 (127×254)	SS	1 (25.4)	
[8]	IM6/937	$[45/0/-45/90]_{ns}$	$n = 3$	Rect.	3×5 (76.2×127)	CC	1 (25.4)	0.67–13.49 (0.31–6.14)
	T800/3900-2	$[45/90/-45/0]_{ns}$				SS		
[15]	AS4/3502	$[45/0/-45/90]_{ns}$	$n = 1$–3	Rect.	5×10 (127×254)	CC	0.5 (12.7)	2.5 (1.13)
						SS		
[13]	Glass/epoxy	$[0_m/90_n]_{ns}$	Many	Sqr.	1.5–5 (38.1–127)	CC	0.5 (12.7)	26 (11.8)
[9]	Glass/epoxy	$[0_m/90_n]_{ns}$	Many	Circ.	7.87–19.68 (200–500)	SS	0. 5 (12.7)	5.06 (2.3)
						CC		
[14]	AS4/3502	$[45/90/-45/0]_{ns}$	$n = 5,6$	Beam	2.16–3.93 (55,100)	SS	0.5 (12.7)	2.92 (1.33)
		$[-45/0/45/90]_{ns}$				CC		

Table 2
Summary of the 8 structural configurations, and corresponding values of critical force and energy

Configuration	Aperture type	Span in. (mm)	Boundary	No. plies	Imp. mass lb (kg)	Critical force lb (N)	Critical energy ft lb (J)
1	Circular	2.5 [63.5]	CC	32	9.92 [4.50]	1805 [8028]	5.63 [7.63]
2	Circular	2.5 [63.5]	SS	32	9.92 [4.50]	1832 [8149]	7.18 [9.73]
3	Square	5.0 [127.0]	CC	32	9.92 [4.50]	1706 [7588]	11.97 [16.23]
4	Square	5.0 [127.0]	SS	32	9.92 [4.50]	1593 [7086]	11.35 [15.39]
5	Circular	2.5 [63.5]	CC	32	20.40 [9.26]	2021 [8989]	6.17 [8.36]
6	Circular	2.5 [63.5]	CC	16	9.92 [4.50]	585 [2602]	1.94 [2.63]
7	Circular	2.5 [63.5]	CC	24	9.92 [4.50]	1091 [4853]	3.47 [4.70]
8	Circular	2.5 [63.5]	CC	40	9.92 [4.50]	2369 [10537]	6.67 [9.04]

large quantity of experimental data gathered during the present investigation, the plots and curves presented in the following paragraphs do not contain the individual data points. Even though only the trend lines obtained by curve fitting the test data or through mathematical models are shown in the following discussion, the complete results are available in previous publications [1,2].

3. Experimental results: five fundamental plots

3.1. Force plot

The peak force curve, such as the one in Fig. 1(a), is divided in the sub and supercritical regimes by the delamination threshold impact energy value, also called critical energy. The peak force recorded during an impact test increases according to a power law curve if a simple spring-mass model is used and as long as no failure occurs in the material. Setting:

$$m\ddot{x} + K_0 x = 0, \tag{1}$$

where m indicates impactor mass, x is the plate surface displacement (neglecting indentation), and K_0 is the pristine (undamaged) structural stiffness, it is possible to obtain the known sine function, which in turn yields the well-accepted equation [17] for peak force, if the assumption of linear elastic response is made:

$$P_{\text{th}}^{\text{peak}} = \sqrt{2K_0 E_{\text{i}}}, \tag{2}$$

where E_{i} is the impact energy, and $P_{\text{th}}^{\text{peak}}$ is the peak theoretical force.

Once the damage threshold is reached, the test data starts deviating from this theoretical value and tends to reach a plateau in correspondence of the Mean Static Ultimate Load (MSUL). It has been previously proposed [1] that the introduction of a non-linear viscous damper, which captures the dynamic damping mechanism associated with the onset of damage and related to the absorbed energy, in a simple spring-mass-dashpot model can greatly improve the accuracy of the prediction. The instantaneous value of the effective peak force is then linearly related to the displacement x through the structural stiffness K_0 and in a non-linear fashion (exponent n) to the impact velocity V (first derivative of the displacement x) through the damping coefficient c.

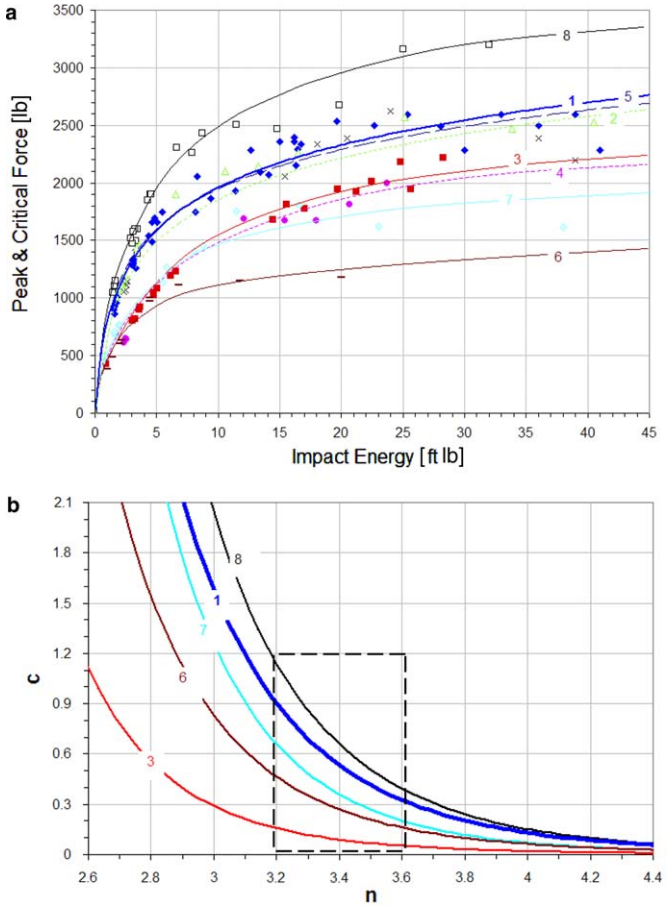

Fig. 1. (a) Force plot for 2 support spans and boundary conditions, 4 laminate thicknesses, and 2 impactor masses. (b) The empirically determined c and n parameters for the spring-mass-dashpot equation for 2 support spans and 4 laminate thicknesses.

$$P_{\text{eff}}^{\text{peak}} = K_0 x + c\dot{x}^n. \tag{3}$$

Setting $V = \sqrt{\frac{2E_{\text{i}}}{m}}$ and solving for the value of the peak force, it is possible to obtain [1]:

$$\begin{aligned} P_{\text{eff}}^{\text{peak}} &= -\frac{c}{2}V^n + \sqrt{2K_0E_{\text{i}} + \frac{c^2V^{2n}}{4}} \\ &= -\frac{c}{2}\left(\frac{2E_{\text{i}}}{m}\right)^{\frac{n}{2}} + \sqrt{2K_0E_{\text{i}} + 2^{n-2}\frac{c^2}{m^n}E_{\text{i}}^n}. \end{aligned} \tag{4}$$

For the reference configuration, 1, the optimum values of the two parameters were previously found to be $n = 3.00$ and $c = 1.54$, however many are the combinations of the two parameters that yield accurate curves in the ranges $n = [3.00, 4]$. The higher the damping coefficient, the lower the non-linear exponent, and vice versa, as shown in Fig. 1(b), therefore satisfying combinations of c and n are the ones which are neither under- nor over-damped. The plot indicates that a decreasing relative structural stiffness has the effect of shifting the curves toward the origin, from configuration 8–3. Furthermore, more compliant, flexural dominated configurations are better described by values of n in the range [3.25–4.25], while stiffer, shear dominated ones are more accurately described by values of n [3.00–3.75]. The range of n between 3.25 and 3.75 seems therefore to be the one of more general accuracy.

The importance of employing a force–energy curve, obtained by means of a spring-mass-dashpot model, is to visualize immediately in what regime a certain impact event stands, with respect to the critical energy/force level and the asymptotic ultimate load. Caution has to be exercised if comparison of impact events is solely based upon peak force, because of its non-linear dependence with impact energy. Secondly, that beyond a certain value of impact energy peak force does not uniquely define the state of damage, even if penetration or perforation does not occur.

The value of the critical force was shown in [1–4,11,18,19] to be independent of impact energy, and comparisons between structural configurations can be performed effectively by using this parameter. Use of a peak force plot such as the one in Fig. 1, in conjunction with the constant value of the critical force, allows for comparing structural configurations in a direct and global manner. It is hence possible to individuate two different stages in the supercritical regime of the force–energy curve: the first, characterized by peak force values progressively deviating from the theoretical power law prediction; and the second, where the peak force has reached an asymptotic value, corresponding to the MSUL, even in the case where no penetration/perforation occurs. All configurations tend to the asymptotic value corresponding to the MSUL.

The plot indicates that curve 3 is located 25% away from curve 1. This difference is not due to the shape of the aperture, since for a quasi-isotropic lay-up and a hemispherical impactor the square and circular configuration maintain the same axial symmetry, but is exclusively related to the aperture size. It is known that support span plays a major role in the low velocity, high mass impact testing of composite targets, due to the global nature of the event, but the advantage of plotting the force–energy curve is to better visualize the global behavior rather than concentrating on a few data-points.

Curve 2 and 4, obtained removing all clamping devices, such as the screws and cover plate, thus providing purely simply supported boundary conditions, are situated 6% apart from the respective curves 1 and 3 in the subcritical regime, and the difference progressively decreases, as they tend to converge to the same asymptotic value. The conventionally adopted practice of firmly clamping composite targets with peripheral screws for impact testing appears to be of little beneficial effect. The reason for the discrepancy with other results [4] can be found in the method employed to provide the clamping effect, whereby a higher degree of clamping can be provided. Nonetheless, the peak force values recorded for clamped specimens is 20–24% greater than for simply supported specimens, which is much less than predicted by plate theory or Finite Element codes (see later section), and has been reported only for a very limited amount of data [4]. Lastly, doubling impactor mass, in this range of high-mass, low-velocity impacts does not seem to have substantial effects on the peak force, as shown by curve 5.

The critical force and critical energy values for the various configurations are recapitulated in Table 2. It can be noted once again that the values for the supported and clamped configurations are extremely close. The small aperture exhibits the same critical force value as the larger one, yet the critical energy threshold is nearly 50% lower. This observation is in agreement with the ones reported in [4,11] which supported the conclusion that the onset of damage is better described by a force rather that energy parameter. On the other hand, the critical force and energy values for the 20.4 lb (9.26 kg) impactor specimens appear to be higher than the 9.92 lb (4.5 kg) impactor, but the discrepancy is due to the inertial oscillations recorded by the instrumentation, which are signal spikes that have no effect on the integrity of the structure.

Nettles and Douglas [5] tried to address the fact that plates having the same span to thickness (s/t) ratio yield do not necessarily behave in the same fashion. However it is hard to draw conclusions from their data since their considerations are based only on the inspection of the load–deflection curves and the peak force values recorded during the event. Plots such as the one in Fig. 1(a), with the aid of design curves such as the one of Fig. 1(b), suggest that a great deal of difference can be expected in the response of structures having the same s/t ratio but different absolute values. As an example, it can be noticed how curves 3 and 6, having both a ratio $s/t = 34.5$, are well apart from each other. Furthermore, even the critical energy and force values differ greatly for configurations 3 and 6, therefore suggesting that the two dimensions are non-linearly related.

3.2. Energy plot

The energy plot, such as the one of Fig. 2, is comprised of the dissipated energy curve, as well as the 1:1 line of available incident kinetic energy. It has been shown in [1,12,20,21] that dissipated energy increases quadratically with impact energy, while the critical energy is independent of the impact energy level at which the test is performed. It has also been shown [12] how dissipated energy relates directly to the amount of damage introduced in the specimen as measured by failure investigation methods such as

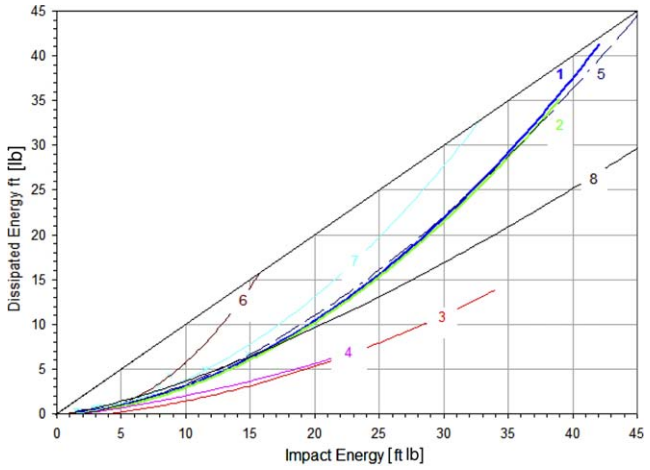

Fig. 2. Energy plot for 2 support spans and boundary conditions, 4 laminate thicknesses, and 2 impactor masses.

ultrasonic and X-ray scans, or microscopic analysis. Hence for the present paper it will be used as a quantitative indication of the general state of damage within the structure. It is furthermore possible to extrapolate, if there exists, the impact energy level at which penetration will occur by forecasting the point of intersection between the quadratic dissipated energy curve and the incident energy line. It has also been shown that dissipated energy curve can be divided in three regimes [20] up to perforation according to the different types of permanent deformation/damage induced in the laminate.

Noting that the dissipated energy is quadratically related to the impact energy [1,12,20], and substituting for the impact velocity, it is possible to obtain:

$$E_D = \varphi E_i^2 = \frac{\varphi m^2}{4} V^4, \tag{5}$$

where φ is a numerical parameter. Since the non-linear dashpot can be described (Eq. (4)) by cV^n, it is possible to obtain:

$$E_D = \int c\dot{x}^n \, dx. \tag{6}$$

The physical meaning of Eq. (6) is that the total work done by the viscous force, associated with the damper that represents damage, is equal to the total energy dissipated during the impact event. A more detailed treatment of the modified spring-mass models can be found in [3].

The energy balance [9] that relates impact energy to the elastic strain energy (E_E) component and the absorbed energy term (E_A), which is a sum of the contributions given by non-conservative forces (E_{NC}), such as friction and slipping at the boundaries, and the energy dissipated (E_D) in the damage creation and propagation is therefore still applicable:

$$E_i = E_E + E_A = E_E + E_{NC} + E_D. \tag{7}$$

While it is not possible to discern the contributions of the different failure mechanisms to the total dissipated energy curve from this kind of investigation, it is nevertheless possible to conclude that the results obtained by testing with a higher-mass impactor and simply supported boundary conditions are not necessarily more conservative than the ones obtained with lighter ones, as suggested by comparisons based on the force plot, at least in this regime of impact velocities up to 4 m/s. Aperture size plays however a major role in the amount of damage, as clearly shown by the 50% difference between the two curves. Doubling the aperture size not only doubles the delamination energy threshold, but it also halves the total dissipated energy. Lastly, the dissipated energy curves 6–8 follow very similar trends, but are shifted to the right for increasing laminate thickness, thus confirming that impact damage resistance is strictly related to this parameter, in a fashion similar to the one suggested by the force plot. The different critical energy values are summarized in Table 2. As previously noted for the force plot, laminates with same s/t ratio do not behave in the same fashion, as it is clearly indicated by the dissipated energy curves 3 and 6, and by the very different values of both damage initiation and penetration thresholds.

3.3. COR plot

The coefficient of restitution (COR) plot, as the one in Fig. 3, has proved to give an immediate estimate of the failure modes occurring in the specimen at different energy levels. The COR of an immovable target can be equivalently defined as the ratio of the exit to the incident velocity, or the square root of the ratio of the exit to the incident energy.

$$\mathrm{COR} = \frac{v_{out}}{v_{in}} = \sqrt{\frac{E_{out}}{E_i}} = \sqrt{\frac{E_i - E_D}{E_i}}. \tag{8}$$

In the subcritical regime it oscillates around a constant value, which is an indicator of the amount of energy dissipated in vibration at the boundaries and permanent

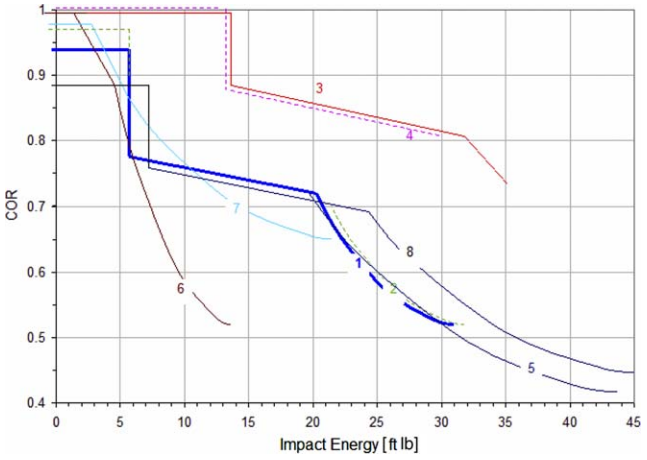

Fig. 3. COR plot for 2 support spans and boundary conditions, 4 laminate thicknesses, and 2 impactor masses.

indentation. At the onset of delamination damage, the curve follows a sharp drop before it becomes constant again; only at much higher impact energy values the COR begins to decrease progressively according to a power law curve. The supercritical regime can therefore be divided in two regions, the first characterized by matrix damage in the form of splitting and delamination, and the second dominated by extensive fiber breakage. In this region the dissipated energy increases at a much faster rate than the kinetic energy available, and eventually, at the perforation threshold, the two quantities will coincide.

The Coefficient of Restitution plot for configurations 1 and 2 is plotted in Fig. 3. The difference in the elastic value of the COR for the each configuration can be attributed to the different amount of energy dissipated during the event. The first cause can be attributed to the different amount of elastic and permanent contact deformation occurring according to the relative stiffness of the target. Secondly, the large overhang of the laminate (up to 1.75 in. per side), clamped underneath the cover plate, which at impact tends to rotate but is contrasted by the steel plate, results in a great energy dissipation mechanism, and again it increases with the relative stiffness of the target.

The critical energy levels for the two apertures show that at failure the COR follows a sharp drop, then decreases with a very gradual slope, being nearly constant over a wide range of impact energy values. A second threshold can be identified, and it indicates the transition from matrix to fiber dominated failure mechanisms [1], beyond which the COR decreases according to a power law curve. It appears that such curve reaches an asymptotic value and then, if there exists, suddenly drops to zero at the penetration threshold. The relative drop in COR due to the onset of delamination is much smaller for the larger span or the thinner laminates, due to the different failure modes that characterize flexible and stiff targets [5]. As previously noted, flexible targets yield a higher value of COR in the subcritical regime, due to either a trampoline effect or a lower amount of energy dissipated at the boundaries or in contact deformation [1], and in the limit the COR is identically equal to unity when these dissipation phenomena are negligible. It can also be noted that, beyond the damage initiation threshold, the amount of energy dissipated in the fracture process greatly exceeds the amount dissipated at the boundaries, and the recorded values for the clamped and supported specimens coincide, further supporting the observation previously made that boundary conditions play a negligible role in the impact response of composite targets.

The delamination damage plateau for the thinner 16 and 24-ply laminates is noticeably shorter than for the thicker 32 and 40-ply laminates. Almost immediately after the damage threshold, the COR begins to decrease at a fast, nearly linear rate. By looking at this plot it appears that increasing laminate thickness, not only increase the critical impact energy level, hence the impact damage resistance of the structure, but also improves its damage tolerance. Thicker plates exhibit a more pronounced delamination plateau, and delamination damage in a structure is known to be more forgiving than macroscopic fiber breakage, at least to an extent [22]. Impactor mass seems to have no effect on the low velocity impact response of composite plates, at least in the regime in discussion.

The great advantage of this plot is that it gives an immediate visualization of the delamination and fiber damage thresholds, which are not obvious from other plots, and whose determination has conventionally required the time consuming procedure of post-failure investigations, such as microscopy and resin burn-off [9]. And from a quantitative standpoint, it allows for an estimate of the relative contribution of the different failure modes to the total dissipated energy, as shown by Eqs. (7) and (8). As an example, the COR curves for configurations 3 and 6 behave in a very different fashion, suggesting that targets having an equal laminate thickness to support span (D) ratio (t/D) yield very different elastic responses, damage mechanisms and threshold values.

3.4. Contact duration plot

The contact duration curve of Fig. 4 is comprised of two regions, delimited by the critical energy level [1]. In the first region, contact duration is constant because it is inversely related to effective structural stiffness, which is a property of the impactor/target system, by means of the well-known relationship:

$$t_c = \pi\sqrt{\frac{m}{K_0}}. \tag{9}$$

As expected, the curves for configurations 1 and 5 follow each other 43% apart throughout the entire range of impact energy values, due to the different impactor weights.

In the subcritical regime, specimens with simply supported boundaries yield a 12% longer duration of impulse,

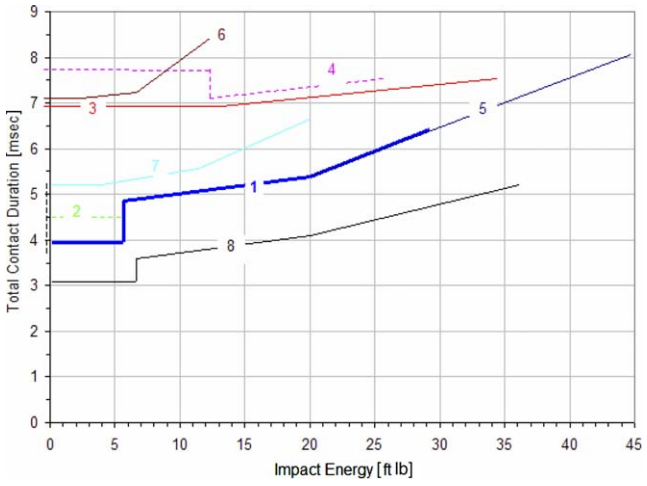

Fig. 4. Contact duration plot for 2 support spans and boundary conditions, 4 laminate thicknesses, and 2 impactor masses.

thus suggesting that such targets behave in a more compliant fashion (3.5%) than the clamped ones. The difference in contact duration due to the boundary condition indicates a difference in effective structural stiffness, which is not captured as clearly by the previous plots. The larger aperture also yields a more compliant configuration, since doubling the support span seems to double the duration of contact.

At the onset of damage it begins to increase almost linearly, thus confirming that the specimen undergoing fracture is becoming more compliant during the impact event, hence the residence time of the impactor on the target is increasing.

In the case of the smaller aperture, contact duration follows a sharp jump and then it gradually increases for increasing values of impact energy. In the case of the larger aperture and thinner laminates, such discontinuity is not evident, but contact duration increases progressively after the onset of damage. The presence of the jump can be possibly used as indicator of the relative stiffness of the target [5,14]. It should be noticed that laminates with same thickness to span ratio don't perform in the same way, since effective structural stiffness is strictly related to both aperture size and plate thickness, as in the case of configurations 1, 3 and 6.

3.5. Residual stiffness plot

Taking advantage of the fact that contact duration is a property of the impactor/target system and, in the elastic regime, is independent of the impact energy level at which the test is performed, and employing the three-test matrix introduced in [1], it is possible to build a residual performance curve. The ratio of pristine to damaged contact duration has been shown to give a direct indication of the residual transverse stiffness of the plate and to allow for the building of a normalized CAI-type curve [13,16,22–26], as the one of Fig. 5.

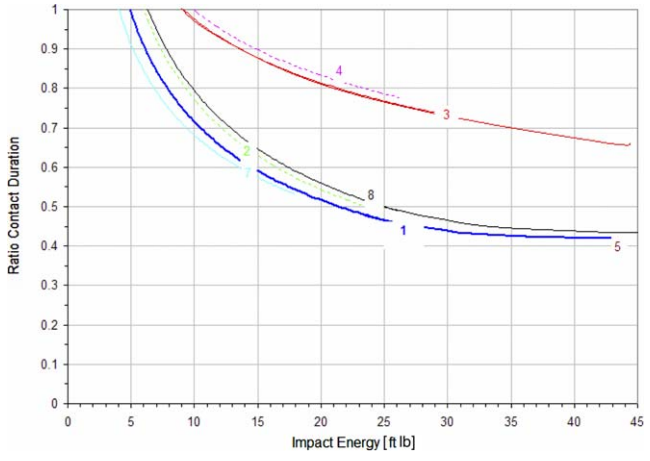

Fig. 5. Residual stiffness (normalized contact duration) plot for 2 support spans and boundary conditions, 4 laminate thicknesses, and 2 impactor masses.

The curve previously obtained for the reference configuration suggests that

$$\frac{t_0}{t_D} = \left(\frac{K_D}{K_0}\right)^{\frac{1}{2}} = \left(\frac{E_C}{E_i}\right)^{\alpha}, \tag{10}$$

where E_i is the impact energy, subscripts 0 and D indicate pristine and damaged values of a certain material property, E_C can be found in Table 2 and the empirical parameter α has a value of 0.5.

A first consideration has to be made with regards to boundary conditions. The curves obtained for supported specimens lie in both cases 7% above the ones for the clamped targets. This is consistent with the observations made so far, that boundary conditions play a minor role in the overall impact performance of composite targets, even at such low impact velocities, and the data shows that the supported configuration values are only slightly less conservative than the clamped ones. The other important conclusion resulting from this plot is that the larger aperture introduces consistently less damage than the smaller aperture. More flexible specimens follow a curve with an α exponent of 0.25, and the value of E_C is about twice as high. Again this observation is consistent with the ones for peak force, dissipated energy and COR. Impactor mass has a negligible influence on the response of a composite target, for this particular range of impact velocities, since the two curves for the 9.92 and 20.4 lb (4.50 and 9.26 kg) impactor weights are nearly identical. Lastly, laminate thickness has little influence on the normalized curves, which exhibit very nearly identical values of the exponent α. Except for the different values of the critical energy E_C, it appears that while laminate thickness plays a major role in the damage resistance characteristics of a structure, it has no beneficial effects on its relative (normalized) damage tolerance, consistently with the conclusions reached by CAI testing [13,22].

4. Numerical results

An ABAQUS© is developed to expand the range of investigation on the effect of structural parameters on the impact response of composite plates. The model employs solid axis-symmetric quadrilateral elements, shown in Fig. 6, and the macroscopic laminate elastic properties are specified as engineering constants (smeared properties) instead of ply-by-ply lamina properties, taking advantage of the relative degree of isotropy and homogeneity of the present configuration.

A quasi-static indentation is obtained by assigning a crosshead speed of 0.05 in/min (1.27 mm/min), while the dynamic model is obtained by assigning the aluminum indenter/impactor a velocity of 55 in/s (1397 mm/s), resulting in impact energy of 3.21 ft lb (4.35 J), which is located in the subcritical regime. To verify that the accuracy of the model in both ranges, the load–time and load–displacement traces are matched to the experimentally determined

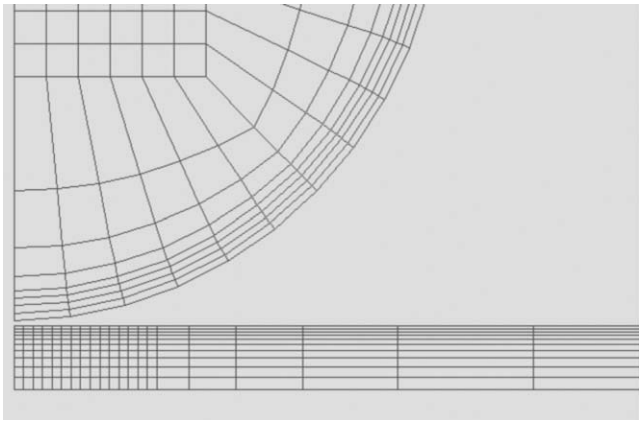

Fig. 6. Mesh and geometry of the Abaqus axis-symmetric model.

ones, focusing in particular on the values of peak-recorded force and contact duration. Simply supported boundary conditions have proved to give the accurate results, consistently with experimental observations, while clamped boundary conditions greatly over-estimate the results. The reason for the discrepency can be found by considering that the radial displacements and tangential rotations are not effectively constrained in this type of experimental setup, and that the supports tend to show a flexible behaviour, particularly for small test apertures.

For the same level of impact energy 3.21 ft lb (4.35 J), the impactor weight and velocity are varied to verify experimental results and previous observations that suggest a great deal of difference in the response of composite plates to mass- or wave-dominated impact events. The weight of the hemispherical impactor is varied by changing the density of the material without affecting the diameter. The iso-energy curve thus obtained, plotted in Fig. 7, shows how quickly the peak-recorded force drops in the range of [0–2] lb, (0–0.9 kg) and then decreases only slightly in the range [3–35] lb (1.4–15.9 kg).

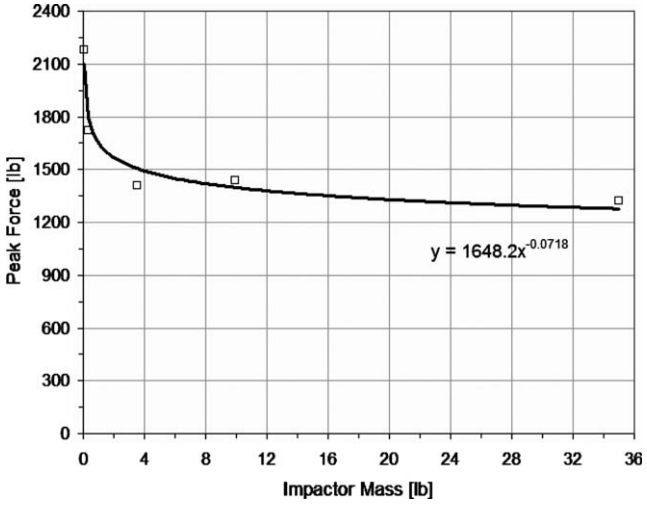

Fig. 7. Estimated influence of impactor weight on peak-recorded force for the same value of impact energy.

On the other hand, the iso-velocity curve of Fig. 8, also obtained analytically by varying the value of density of the impactor without affecting its size, closely follows the iso-mass curve obtained experimentally. However, the slightly higher values of the peak force predicted are consistent with previous observations that suggest how the nature of high-velocity (or wave dominated) events is more localized, and the resulting stiffening mechanism yields higher contact forces. Depicted in Fig. 9 is the numerical power law curve that relates contact duration to impactor weight [1], and confirms the Eq. (9) derived from the spring-mass model.

Parameters such as support span, laminate thickness and in-plane (equivalent) laminate modulus have been varied, and the results can be summarized by the existing equation for effective structural stiffness K_0 [17]:

$$K_0 = \frac{4\pi E_r h^3}{3(1-\nu^2)R^2}, \tag{11}$$

where R is aperture radius, h is laminate thickness, E_r and ν are in-plane average modulus and Poisson's ratio of the laminate. While damage initiation and penetration resistance properties of the target are known to greatly depend on impactor characteristics [20–24], such as size and material, Eq. (11) does not describe the influence of impactor properties on the elastic response of composite plates. Impactor diameter and elastic modulus are found to influence the response of a composite plate in this range of impact events. Varying the modulus of the impactor while maintaining linear elastic material assumption, as shown in Figs. 10 and 11, causes an increase up to 20% in the value of peak force and contact duration. Similarly, the plots depicted in Figs. 12 and 13 suggest a consistent relationship between impactor diameter and peak force and contact duration. Observing that: $t_c \propto E_t^{-0.04}$ and $t_c \propto d_t^{-0.08}$ it is possible to obtain the following:

$$K_0^{tup} = \varphi \frac{d_t^{16/100} \cdot E_t^{8/100}}{m^{8/100}}, \tag{12}$$

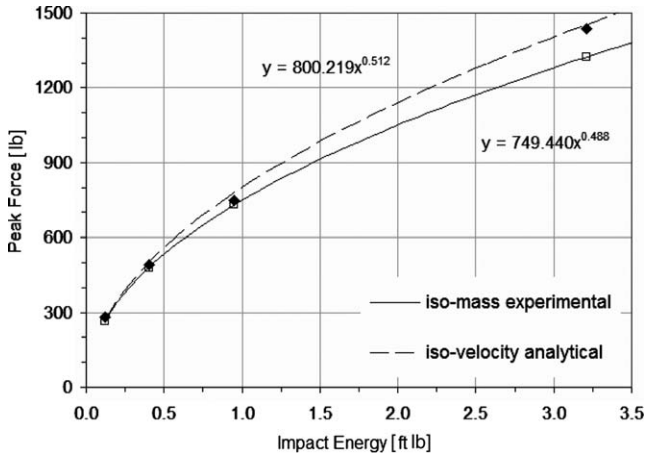

Fig. 8. Comparison between analytical and experimental data in the force–energy curve (subcritical regime only).

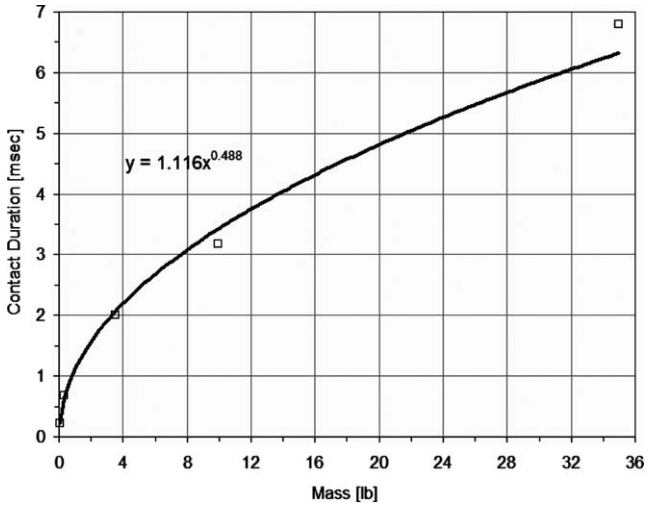

Fig. 9. Dependence of contact duration on impactor weight.

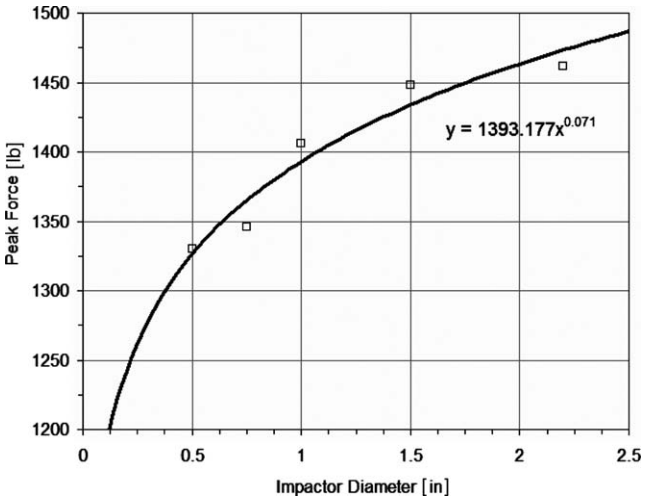

Fig. 12. The peak force depends on impactor's size.

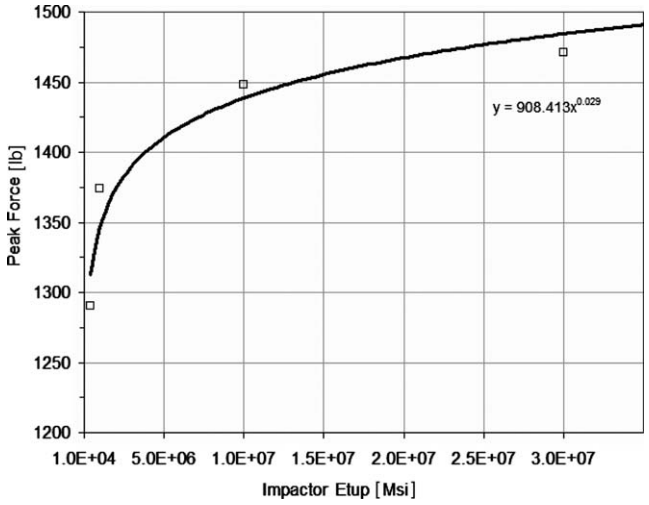

Fig. 10. The value of peak force depends on the impactor's elastic modulus.

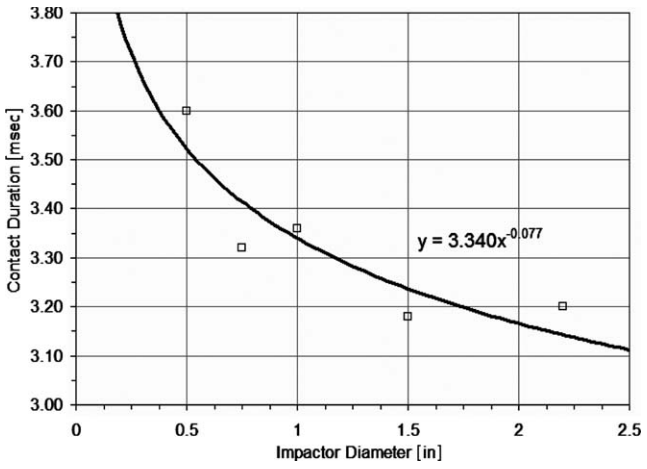

Fig. 13. Abaqus plot indicating that the elastic value of contact duration depends on impactor's size.

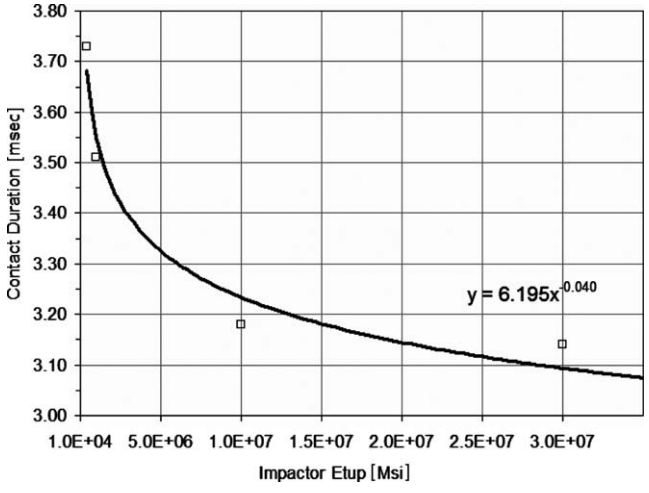

Fig. 11. The elastic value of contact duration is a function of the impactor's elastic modulus.

where E_t, m and d_t are impactor modulus, weight and diameter, respectively, while φ is a numerical constant. The non-dimensional term introduced here captures the dynamics of the impact event associated with the characteristics of the impactor. The effective structural stiffness of the target from Eq. (11) can be therefore described as:

$$K_0^{\text{eff}} = \varsigma \cdot \left(\frac{E_r}{1-\nu^2}\right) \cdot \left(\frac{h^3}{R^2}\right) \cdot \left(\frac{d_t^2 \cdot E_t}{m}\right)^{2/25}, \tag{13}$$

where ζ is a numerical parameter, and the three terms in parentheses are the target material, target geometry and impactor components, respectively. As an example, for $d_t = 1.5$ in. (38.1 mm), $E_t = 10$ Msi (69 GPa), $m = 10$ lb (4.5 kg), Eq. (12) is equal to 1.07, for $d_t = 0.5$ in. (12.7 mm), $E_t = 30$ Msi (207 GPa), $m = 0.5$ lb (0.23 kg), Eq. (12) yields 1.24, while for $d_t = 0.5$ in. (12.7 mm), $E_t = 10$ Msi (69 GPa), $m = 4$ lb (1.8 kg), Eq. (12) equals 0.96. The latter term appears to be less influent than the target

characteristics terms, at least in the velocity regime used in this type of investigation. However, while Eq. (11) loses validity in the high-velocity, low-mass regime, Eq. (13) provides a more general means by which to describe the impact event, independently from the impact velocity regime.

5. Conclusions

Durability and damage tolerance design methodologies must address the deleterious effects associated with changes in material properties and the loss of structural integrity that may occur during the service lifetime of a vehicle, and therefore need to rely on extensive and costly experimental databases. A comparison of impact events on a composite structure performed exclusively on the basis of the recorded peak force, damage area or residual strength of a composite target can be limiting. The importance of characterizing an event by means of multiple parameters has been shown, and a novel Composite Structure Impact Performance Assessment Program (CSIPAP) has been proposed. It is comprised of three consecutive impact tests per specimen, two elastic and one to introduce damage. The data obtained can be processed so that comparisons between structural configurations can be performed on the simultaneous investigation of the Force, Energy, Coefficient of Restitution (COR), and Residual Stiffness (normalized contact duration) plots. Only a combined approach as the one here suggested allows the designer to immediately visualize the overall performance of each target and, more importantly, to benefit from the greater insight that can be gained by performing a structural comparison based on over multiple parameters.

The results previously obtained [1] for the prediction of the force–energy and residual stiffness curves have proved to apply to the configurations tested, therefore confirming their general validity. Examples of how such program can be applied to determine the relative influence of impactor/target parameters on the impact response of composite plates have been provided. Results have shown that conventional clamping devices used in low-velocity impact testing, as well as aperture shape have little effect on the impact response of a composite target, and it is therefore possible to perform comparisons among different configurations across the existing literature. On the other hand, support span and laminate thickness have a significant effect on the impact event, as do impactor size and modulus, whose influence has been previously neglected.

Acknowledgements

The authors express their gratitude to Wade C. Jackson and T. Kevin O'Brien (Army Research Laboratories at NASA Langley Research Center) for providing invaluable discussions during the development of the study. Paolo express his gratitude to the American Society for Composites (ASC) for having bestowed upon him the 2004 Ph.D. Research Award for the present work. Lastly, the corrections suggested by two anonymous reviewers greatly contributed to the improvement of the paper. *Per aspera astra ad ulteriora*.

References

[1] Feraboli P, Kedward K. Enhanced evaluation of the low velocity impact response of composite plates. AIAA J 2004;42/10:2143–52.
[2] Feraboli P, Kedward K. A multi-parameter approach to impact performance characterization. In: 19th ASC/ASTM Joint Technical Conference; 2004.
[3] Feraboli P. Modified SDOF models for improved representation of the impact response of composite materials. J Compos Mater (2006).
[4] Jackson WC, Poe CC. The use of impact force as a scale parameter for the impact response of composite laminates. J Compos Technol Res, 15/4, Winter; 1993. p. 282–9.
[5] Nettles AT, Douglas MJ. A comparison of quasi-static indentation to low-velocity impact, NASA TP-2000-210481, Aug.; 2003.
[6] Ambur D, Kemmerly HL. Influence of impactor mass on the damage characteristics and failure strength of laminated composite plates. In: 39th AIAA/ASME/ASCE/AHS/ASC structures, structural dynamics and materials conference, No. 98-1784; 1998.
[7] Prasad CB, Ambur DR, Starnes JH. Response of laminated composite plates to low speed impact by different impactors. AIAA J 1994;32(6):1270–7.
[8] Ambur DR, Starnes JH, Prasad CB. Influence of impact parameters on the response of laminated composite plates. In: Martin RH, editor. ASTM STP 1230; 1995. p. 389–404.
[9] Delfosse D, Poursartip A. Energy-based approach to impact damage in CFRP. Compos Part A 1997;28A:647–55.
[10] Li CF, Hu N, Cheng JG, Fukunaga H, Sekine H. Low velocity impact induced damage of continuous fiber-reinforced composite laminates. Part II. Verification and numerical investigation. Compos Part A 2002;33:1063–72.
[11] Sjöblom P. Simple design approach against low velocity impact damage. In: 32nd international SAMPE symposium; 1987. p. 529–39.
[12] Sjöblom P, Hartness T, Corbell TM. On low velocity impact testing of composite materials. J Compos Mater 1988;22(1):30–52.
[13] Zhou G. Effect of impact damage on the residual compressive strength of glass–fibre reinforced polyester (GFRP) laminates. Compos Struct 1996;35:171–81.
[14] Liu D, Raju BB, Dang X. Size effects on impact response of composite laminates. Int J Impact Eng 1998;21(10):837–54.
[15] Lifschiz JM, Gov F, Gandelsman M. Instrumented low-velocity impact of CFRP beams. Int J Impact Eng 1995;16(2):201–15.
[16] Kistler LS, Waas AM. Experiment and analysis on the response of curved laminated composite panels subjected to low velocity impact. Int J Impact Eng 1998;21(9):711–36.
[17] Shivakumar KN, Elber W, Illg W. Prediction of Impact force and duration due to low-velocity impact on circular composite laminates. J Appl Mech 1985;52:674–80.
[18] Belingardi G, Vadori R. Low velocity impact tests of laminate glass fiber epoxy matrix composite material plates. Int J Impact Eng 2002;27:213–22.
[19] Schoeppner GA, Abrate S. Delamination threshold loads for low velocity impacts on composite laminates. Compos Part A 2000;31:903–15.

[20] Liu D, Raju BB. Effects of bending-twisting coupling on impact resistance of composite laminates. In: 18th A.S.C. technical conference; 2003.
[21] Tomblin J, Suresh Raju K, Arosteguy G. Damage resistance and tolerance of composite sandwich panels – scaling effects – DOT/FAA AR-03/75. Feb.; 2004.
[22] MIL-HDBK-17-3F: vol. 3 – Damage resistance, durability and damage tolerance [chapter 7].
[23] Hahn HT, Mitrovic M, Turkgenc O. The effect of loading parameters on fatigue of composite laminates: part III, DOT/FAA/AR-99/22, June: 1999.
[24] Shyprykevich P, Tomblin J, Ilcewicz L, Vizzini AJ, Lacy TE, Hwang Y. Guidelines for analysis, testing, and nondestructive inspection of impact-damaged composite sandwich structures – DOT/FAA AR-02/121, March; 2003.
[25] Caprino G, Lopresto V. The significance of indentation in the inspection of carbon fibre-reinforced plastic panels damaged by low velocity impact. Compos Sci Tech 2000;60:1003–12.
[26] Caprino G, Langella A, Lopresto V. Indentation and penetration of carbon fibre reinforced plastic laminates. Compos Part B 2003;34(4):319–25.